High-Quality Double-Walled Carbon Nanotubes Grown by a Cold-Walled Radio Frequency Chemical Vapor Deposition Process

Alexandru R. Biris,*,† Dan Lupu,† Alexander Grüneis,‡ Paola Ayala,‡,§ Mark H. Rümmeli,‡ Thomas Pichler,‡ Zhongrui Li,∥,⊥ Yang Xu,∥,⊥ Ioan Misan,† Enkeleda Dervishi,∥,⊥ and Alexandru S. Biris*,∥,⊥

National Institute for Research and Development of Isotopic and Molecular Technologies, P.O. Box 700, R-400293 Cluj-Napoca, Romania, IFW−Dresden, Helmholtzstrasse 20, 01069 Dresden, Germany, Helsinki University of Technology, P.O. Box 1000, 020400, Espoo, Finland, and Nanotechnology Center and Applied Science Department, University of Arkansas at Little Rock, Little Rock, Arkansas 72204

Received December 25, 2007. Revised Manuscript Received March 10, 2008

High-quality double-walled carbon nanotubes were synthesized by radio frequency (cold-walled) catalytic chemical vapor deposition from methane on a novel Fe−Mo/MgO catalyst obtained by coprecipitation. Transmission electron microscopy observations provided compelling evidence for the formation of double-walled carbon nanotubes, while the Raman results supported the overall quality of the samples and showed clearly defined radial breathing mode signals corresponding to tubes with diameters ranging between 0.72 and 2.42 nm. The second-order Raman (2D) band was found to be composed of two overlapping peaks corresponding to the inner and outer nanotubes. Thermogravimetric analysis showed a 95% purity for the as-grown material corresponding solely to nanotubes. It was found that inductive heating by a radio frequency source considerably suppressed the deposition of amorphous carbon, leading to very pure samples suitable for further investigations.

Introduction

Double-walled carbon nanotubes (DWCNTs) have attracted a considerable amount of scientific interest due to their unique structural, optical, mechanical, and electronic properties. Their structure allows not only for the study of interwall interactions but also the development of applications where only the external wall is exposed to functional processes, keeping the inner wall pristine and unaltered.[1] Because of the increasing number of applications in a large number of areas that include energy,[2] advanced materials,[3] field emission,[4,5] and conductive films/electrodes of nanoelectronic devices[6,7] that were developed around these types of nanotubes, new efforts have been centered on developing processes to grow high-quality DWCNTs. Some of the early methods included the filling of single-walled carbon nanotubes with fullerenes[8] or metallocenes via thermal treatment. However, these routes resulted in an incomplete and nonuniform filling of the outer tube along its entire length. Some of the most promising synthesis methods include electric arc discharge and catalytic chemical vapor deposition (cCVD).[9,10] A major shortcoming of these latter methods is the difficulty of growing only pristine DWCNTs and not a mixture of DWCNTs and SWCNTs. The reasons for the formation of such mixtures are the very similar catalytic growth conditions of the two species[11] and the inability to control catalytic metal particle sizes, which is essential for tube diameter control. Major developments in the synthesis of DWCNTs have been reported,[12,13] but major research is still needed to obtain high-efficiency catalytic systems that generate crystalline DWCNTs with low levels of other types of nanotubes such as single walls or triple walls. Ago et al.[14] proved the role of strong metal−support interactions in the formation of small-sized metal nanoparticles to be suitable for SWCNT (DWCNT) synthesis over Fe/MgO catalysts.

* Corresponding authors. (A.R.B.) E-mail: biris@oc1.itim-cj.ro; tel.: +040-264-584037. (A.S.B.) E-mail: asbiris@ualr.edu; tel.: +501-749-9148.
† National Institute for Research and Development of Isotopic and Molecular Technologies.
‡ IFW−Dresden.
§ Helsinki University of Technology.
∥ Nanotechnology Center, University of Arkansas at Little Rock.
⊥ Applied Science Department, University of Arkansas at Little Rock.

(1) Flahaut, E.; Bacsa, R.; Peigney, A.; Laurent, C. *Chem. Commun. (Cambridge, U.K.)* **2003**, 1442–1443.
(2) Wei, J.; Jia, Y.; Shu, Q.; Gu, Z.; Wang, K.; Zhuang, D.; Zhang, G.; Wang, Z.; Luo, J.; Cao, A.; Wu, D. *Nano Lett.* **2007**, *7*, 2317–2321.
(3) Baughman, R. H.; Cui, C.; Zakhidov, A. A.; Iqbal, Z.; Barisci, J. N.; Spinks, G. M.; Wallace, G. G.; Mazzoldi, A.; Rossi, D. D.; Rinzler, A. G.; Jaschinski, O.; Roth, S.; Kertesz, M. *Science (Washington DC, U.S.)* **1999**, *284*, 1340–1344.
(4) Buldum, A.; Lu, J. P. *Phys. Rev. Lett.* **2003**, *91*, 236801.
(5) Mayer, A.; Miskovsky, N. M.; Cutler, P. H.; Lambin, Ph. *Phys. Rev. B: Condens. Matter Mater. Phys.* **2003**, *68*, 235401.
(6) Li, Z.; Kandel, H. R.; Dervishi, E.; Saini, V.; Biris, A. S.; Biris, A. R.; Lupu, D. *Appl. Phys. Lett.* **2007**, *91*, 53115.
(7) Misewich, J. A.; Martel, R.; Avouris, P.; Tsang, J. C.; Heinze, S.; Tersoff, J. *Science (Washington DC, U.S.)* **2003**, *300*, 783–786.
(8) Bandow, S.; Takizawa, M.; Hirahara, K.; Yudasaka, M.; Iijima, S. *Chem. Phys. Lett.* **2001**, *337*, 48–54.
(9) Grüneis, A.; Rümmeli, M. H.; Kramberger, C.; Barreiro, A.; Pichler, T.; Pfeiffer, R.; Kuzmany, H.; Gemming, T.; Büchner, B. *Carbon* **2006**, *44*, 3177–3182.
(10) Li, W. Z.; Wen, J. G.; Sennett, M.; Ren, Z. F. *Chem. Phys. Lett.* **2003**, *368*, 299–306.
(11) Muramatsu, H.; Hayashi, T.; Kim, Y. A.; Endo, M.; Terrones, M.; Dresselhaus, M. S. *J. Nanosci. Nanotechnol.* **2005**, *5*, 404–408.
(12) Endo, M.; Muramatsu, H.; Hayashi, T.; Kim, Y. A.; Terrones, M.; Dresselhaus, M. S. *Nature (London, U.K.)* **2005**, *433*, 476.
(13) Flahaut, E.; Bacsa, R.; Peigney, A.; Laurent, C. *Chem. Commun. (Cambridge, U.K.)* **2003**, 1442–1443.
(14) Ago, H.; Nakamura, K.; Uehara, N.; Tsuji, M. *J. Phys. Chem. B* **2004**, *108*, 18908–18915.

10.1021/cm703680n CCC: $40.75
Published on Web 05/06/2008

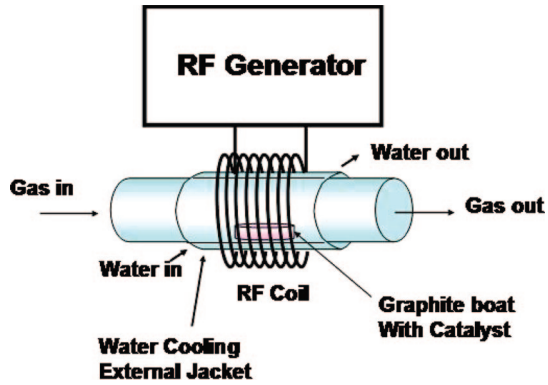

Figure 1. Cold-walled RF-cCVD reactor schematic. The coil induced heat only in the graphite receptacle that holds the catalyst powder, while the external walls of the reactors were continuously water-cooled.

MgO has proven to be a very attractive support since it is easily removed from the final product by washing with nonoxidizing acids such as HCl, which do not damage the structure and morphology of the nanotubes.[15] Yan et al.[16] found that the MgO-supported catalysts prepared by coprecipitation were more effective for SWCNT synthesis than those prepared by the more widely used impregnation method since it gave better control over the size and dispersion state of the catalyst nanoparticles. On the basis of these findings and on the known synergetic effect of Mo, which prevents the agglomeration of catalytic metal nanoparticles on the oxide support by stabilizing the small-sized nanoparticles needed for SWCNT synthesis,[17] the present study aims to develop and study a novel Fe−Mo/MgO catalyst system, which has not previously been reported and can be effectively used for synthesizing high-quality and large quantities of DWCNTs by radio frequency (RF)-cCVD, a method previously developed in our laboratories.[18,19]

Experimental Procedures

A novel catalyst with the composition Fe/Mo/MgO (1:0.2:12.6 wt %) was prepared by coprecipitation as follows. The corresponding quantities of $Mg(NO_3)_2 \cdot 6H_2O$ and $Fe(NO_3)_3 \cdot 9H_2O$ salts were dissolved in ethanol, followed by the slow addition of a solution of $(NH_4)_6Mo_7O_{24} \cdot 4H_2O$ dissolved in NH_4OH (25%) under continuous stirring. After 24 h, the precipitate was filtered and dried at 150 °C for 2 h and calcinated at 500 °C for 1 h. The final catalyst had the appearance of a beige fluffy powder.

The carbon nanotubes synthesis was performed by RF-cCVD—a method already presented previously.[18,19] Approximately 100 mg of catalyst was distributed uniformly over the flat bottom of a graphite receptacle (10 cm length and 1.95 cm width), which was introduced in a horizontal 20 mm diameter and 800 mm length quartz tube, and placed in the middle of a copper-cooled coil connected to a high-frequency generator (5 kW, 1.9 MHz), as shown in Figure 1. A second quartz tube of a slightly larger (1 cm) diameter was placed over the outside wall of the quartz reactor, and water was continuously flowed between the reaction reactor and the exterior jacket represented by the larger diameter quartz tube. In this way, the outside wall of the cCVD reactor was always cooled, and therefore, the only hot components of the process were the graphite receptacle and the catalyst system, due to the inductive RF heating. In this process, a significant temperature gradient (550 °C/cm) between the catalyst and the reactor walls was measured. Since the heat was induced directly in the graphite receptacle, the temperature variations between the two ends and the middle of the receptacle were found to be below 1 °C, as measured by high-resolution infrared thermometry. Such low temperature variations were therefore expected to ensure highly uniform nanotube synthesis along the entire area of the receptacle. After flushing the reactor with argon (Ar) (600 mL/min) for 15 min, the crucible containing the catalyst system was heated inductively to 850 °C with a heating rate of 350 °C/min, followed by the administration of a mixture of methane (180 mL/min) and hydrogen (20 mL/min) throughout the reaction process (30 min). The pressure inside the reactor was not found to increase above the atmospheric pressure during the experiments. At the end of the synthesis, the carbon source and hydrogen were stopped, and the graphite crucible was allowed to cool to room temperature in Ar.

Throughout the reaction, the temperature was kept constant and monitored by an infrared thermometer (Impac, IGA 8 plus). Blank experiments (without catalyst) did not show the evidence of nanotubes or any other carbonaceous products being grown. The efficiency (η) of the carbonaceous product that resulted after each synthesis was calculated according to the formula:

$$\eta\,(\%) = [(m_{ar} - m_b)/m_{br}] \times 100\% \qquad (1)$$

where m_{ar} is the mass of the sample after the synthesis, m_{br} is the mass of the catalyst before the reaction, and m_b is the mass of the catalyst after the blank experiments.[20] The as-prepared nanotubes obtained after the growth process (denoted as AP) were purified by using hot Soxhlet extraction with HCl (1:1) for 24 h. To not destroy the tube crystallinity due to the acidic treatment of the catalysts, the nanotubes were kept in water, and the acid was gradually added followed by an increase in temperature. A final washing also was done in the Soxhlet apparatus with distilled water for 24 h. The water was continuously changed until the resulting pH of the solution became neutral. Finally, the nanotubes were filtered and dried overnight at 120 °C. From this point, these samples will be called SE. In a second purification step, the SE product was oxidized in air at 450 °C (heating rate of 10 °C/min) for 20 min, sonicated in HCl (1:1) for 30 min, filtered, washed, and dried at 120 °C overnight. These samples are labeled as OX.

For a thorough structural and morphological examination, all samples were analyzed by scanning and transmision electron microscopy (SEM and TEM), Raman and UV−vis-NIR spectroscopy, and thermogravimetric analysis (TGA). TEM micrographs were recorded with a high-resolution analytical TEM Tecnai F30-300 kV (FEI). For this analysis, carbon nanotubes were dispersed in 2-propanol and ultrasonicated for 10 min. A few drops of the suspension were deposited on the TEM grid and then dried before analysis. Raman scattering studies were performed at room temperature with three laser excitations: 514 nm (2.41 eV), 633 nm (1.96 eV), and 1064 nm (1.16 eV). For the 514 and 633 nm excitations, a Horiba Jobin Yvon LabRam HR800 spectrometer equipped with a charge-coupled detector and two grating systems (600 and 1800 lines/mm) was used. The laser beam intensity

(15) Flahaut, E.; Peigney, A.; Laurent, C.; Rousset, A. *J. Mater. Chem.* **2000**, *10*, 249–252.
(16) Yan, H.; Li, Q.; Zhang, J.; Liu, Z. *Carbon* **2004**, *40*, 2693–2698.
(17) Alvarez, W. E.; Kitiyanan, B.; Borgna, A.; Resasco, D. E. *Carbon* **2001**, *39*, 547–558.
(18) Lupu, D.; Biris, A. R.; Jianu, A.; Bunescu, C.; Burkel, E.; Indrea, E.; Mihăilescu, G.; Pruneanu, S.; Olenic, L.; Misan, I. *Carbon* **2004**, *42*, 503–507.
(19) Biris, A. R.; Biris, A. S.; Lupu, D.; Trigwell, S.; Dervishi, E.; Rahman, Z.; Mărginean, P. *Chem. Phys. Lett.* **2006**, *429*, 204–208.
(20) Méhn, D.; Fonseca, A.; Bister, G.; Nagy, J. B. *Chem. Phys. Lett.* **2004**, *393*, 378–384.

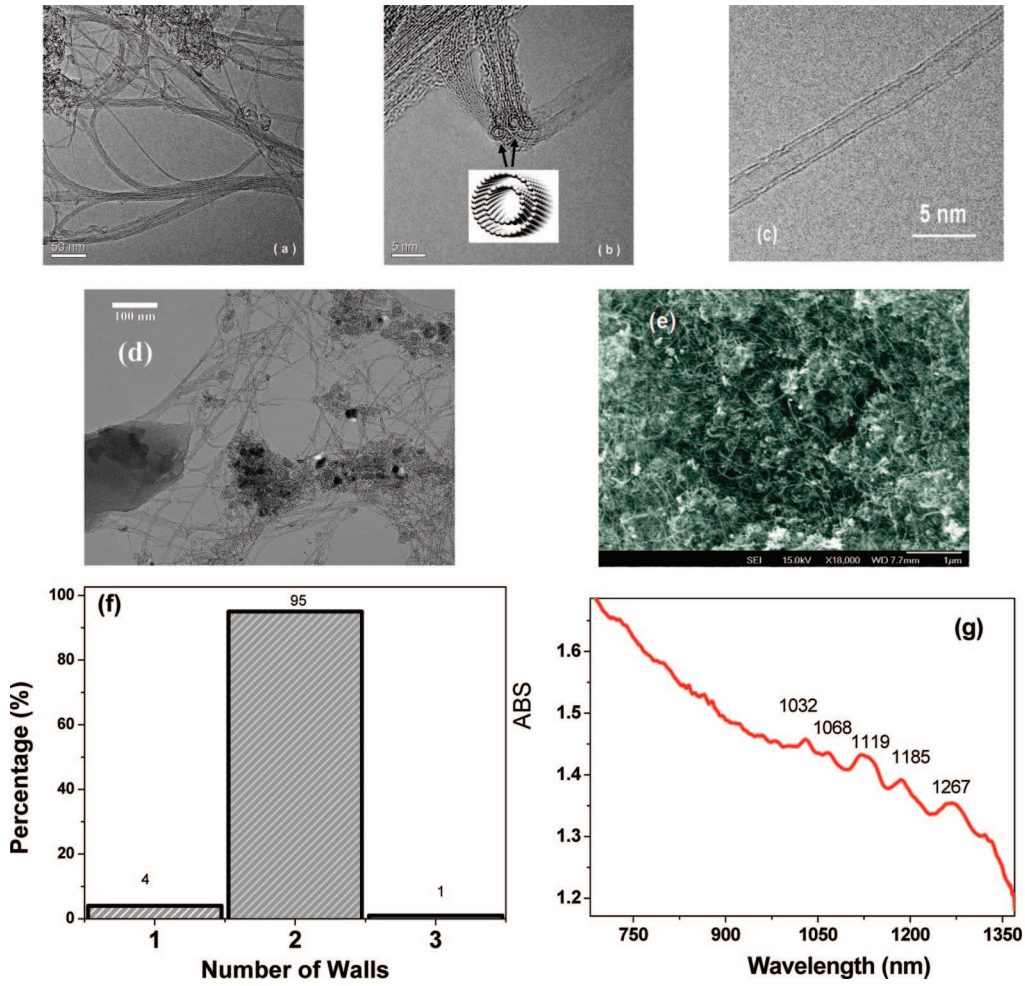

Figure 2. Low (a) and high (b and c) magnification TEM analysis of the DWCNTs obtained by RF-cCVD over the Fe−Mo/MgO catalytic system with methane as a carbon source after purification. Some imperfections present on the walls of the nanotubes shown in panel c are believed to have been induced during the measurement process. Panels d and e show low-magnification TEM and SEM analyses of the sample before purification. Panel f shows the ratio between various nanotube types present in the sample (after 100 nanotubes were analyzed) with 95% being double walls and small amounts of single walls (4%) and extremely rare triple walls. Panel g shows the optical absorption properties of the double-walled nanotube sample.

measured at the sample was kept at 5 mW. An Olympus microscope focused the incident beam to a spot size of >1 μm^2, and the backscattered light was collected 180° from the direction of incidence. Raman shifts were calibrated on a silicon wafer at the 520 cm^{-1} peak. For the 1064 nm (1.16 eV) excitation, the Raman spectra were recorded with a Bruker FT-Raman spectrometer. TGA was performed between 25 and 850 °C with a TGA Mettler Toledo 815e in air (150 mL/min) at a heating rate of 5 °C/min. A Shimadzu UV-3600 spectrometer with an optical range of 185−3300 nm was used to analyze the optical absorption of the nanotube samples. The spectrometer has three detectors (GaAs, PbS, and PMT) to provide a high sensitivity over an extended spectral range with a resolution of 0.1 nm. For the UV–vis–NIR measurements, 1 mg of DWCNTs was dispersed into 5 mL of a 1 wt % sodium cholate deionized water solution. After 1 h of sonication and 3 h of high-speed (13 000 rpm) centrifugation, a uniform and stable carbon nanotube suspension was produced and was used for the analysis. The measurements were performed at room temperature in 10 mm path length quartz cells.

Results and Discussion

The surface area of the catalyst measured by krypton adsorption was 108 m^2/g after calcination at 500 °C and 24.2 m^2/g after 2 min at 850 °C in Ar. The efficiency of the DWCNT growth process was found to be around 50 ± 2%, which indicates that during each reaction, 100 mg of catalyst produced roughly 50 mg of nanotubes. The synthesis of carbon nanotubes under RF excitation has been previously shown[18,19] to generate nanotubes of very high crystallinity and also with low amounts of amorphous carbon, which is suspected to be responsible for poisoning the nanotube synthesis catalytic reactions. The low level or amorphous carbon produced during the catalytic process can be explained by the formation of skin currents (eddy currents) in the metallic nanocatalysts, which can induce a more efficient carbon conversion into graphitic layers. Moreover, the fact that only the crucible holding the catalyst is heated at the reaction temperature of 850 °C and that the reactor walls are cold can also explain the lower thermal decomposition of the carbon source into noncrystalline carbon species and the growth of nanotubes of high quality. Further investigations are underway.

TEM images obtained for the SE samples are shown in Figure 2a, indicating the presence of bundles with diameters ranging from 10 to 40 nm and individual nanotubes with an exterior diameter of approximately 2 nm and a length of at least 10 μm. Although some TEM images showed the

presence of noncrystalline carbon, no significant amounts (under 0.1−0.5 wt % as resulted from TGA analysis) of such amorphous carbon were observed either on the surface of the bundles or on the surface of the individual nanotubes. No significant correlation between the amount of amorphous carbon detected by TGA and the amount of amorphous carbon detected by TEM was observed in this work. This statement can be explained by the fact that TGA mostly provides information on the overall thermal behavior of the sample (usually several milligrams), while TEM can only focus on and analyze individual nanotubes. Therefore, even if TEM detects small traces of amorphous carbon, it might be localized at the site that is analyzed while the overall quantity of the noncrystalline carbon could be very low.

The high-resolution TEM micrographs shown in Figure 2b prove the existence of DWCNTs (concentric circles). In this example, the outer diameter is 2.15 nm, and the inner diameter is 1.4 nm. Figure 2c shows a DWCNT with diameters of 2.35 and 1.64 nm for the outer and the inner walls, respectively. Low-magnification TEM and SEM images of the nanotubes as produced are shown in Figure 2d,e. The nanotubes have a high aspect ratio, and the coverage of the catalyst particles with nanotubes is uniform. After analyzing 100 nanotubes, it was found that less than 5% of the nanotubes has one or three walls, and no nanotubes with more than three walls were observed, as indicated in Figure 2f. Therefore, this study indicates that besides the DWCNTs, the second nanotube type is represented by the single walls, an observation that can be explained by the very similar synthesis conditions of these two nanotube species. Nevertheless, the catalyst shows a strong selectivity toward growing DWCNTs.

During the cCVD process, CNTs are produced from thermal decomposition of carbon-containing molecules over the surface of carefully chosen transition metal catalysts. The carbon atoms diffuse over the catalyst surface as well in bulk to form a tubular structure that grows from the circumference of the catalyst. The solubility of the metal particle in carbon is controlled by particle size and growth temperature. The supersaturation of the metal nanoparticles with carbon results in the precipitation of solid carbon, which subsequently builds the nanotube structure.[21,22] It is possible that the Fe nanoparticles are individually dispersed onto the larger Mo nanoparticles present on the surface of the MgO support, as previously shown.[23] The element Mo probably plays two different roles in the CNT synthesis. First, Mo can act as a secondary support for the active metal such as Fe here. The active metal particles docked on the relatively larger Mo particles, which were supported by MgO powders.[24] Second, Mo can also participate in the breakup of the hydrocarbon molecule and be responsible for a more efficient carbon source conversion, which is reflected in a higher yield for nanotube growth.[25] It has been reported that the use of a conditioning catalyst such as Mo/Al_2O_3[26] caused more DWCNTs than SWNTs to grow, possibly because of an increase in the amount of the active carbon species.[27] Carbon-containing radicals are much more active for the carbon tube formation since they greatly reduce the reaction potential. Because a direct correlation is believed to exist between the size of the active metal nanoparticles (Fe and Mo) forming the nanotubes and the diameters and types of the corresponding nanotubes,[28] this catalytic system was found to show a strong selectivity toward the synthesis of DWCNTs.

Figure 2g shows the optical absorption of the nanotube samples in different spectral ranges. Different environments surrounding the CNTs will influence their optical properties and activity. Therefore, the dispersant used for the solubilization of the nanotubes is critically important. The optical absoprtion peaks corresponding to the outer walls of the DWCNTs that are in contact with the sodium cholate surfactant were shown to present a red shift (about 13 meV) as compared to the case when they were dispersed in sodium dodecyl sulfate solution.[29] An empirical Kataura plot was used to assign the DWCNT structure species in aqueous solution (calculated as a reference to the sodium cholate solution).[30] The first van Hove transition (S_{11}) wavelengths at 1267, 1185, 1119, 1068, and 1031 nm can be assigned to specific semiconducting nanotubes with diameters of 1.0−0.8 nm, which belong to (8, 7), (12, 1), (8, 4), (10, 2), and (7, 5) chiral groups. The corresponding second van Hove transitions (S_{22}) peaks at 730, 800, 590, 738, and 643 nm were not very dominant. These five wavelength peaks were assigned to the larger outer diameter nanotubes, (20, 6), (14, 12), (16, 9), (15, 7), and (12, 10), which belong to the second van Hove transitions (S_{22}') as they covered the 1.5−2.4 nm range of the outer diameter DWCNTs. This analysis indicated that the DWCNT samples have relatively narrow diameter distributions.

Figure 3 presents the TGA curves for the DWCNTs as synthesized (panel a) and analyzed after each of the two stages of purification (panel b). The inset shows the corresponding differential thermal analysis (DTA) curves. Their minimal positions relative to the temperature axis represent the burning (thermal decomposition) temperatures.[31,32]

The thermal disintegration curves show one mass loss profile and reflect the existence of a single carbonaceous product, even for the as-produced samples (Figure 3a).[33] The mass increase in the temperature range of 450−520 °C

(21) Charlier, J.-C.; Iijima, S. *Top. Appl. Phys.* **2001**, *80*, 55–80.
(22) Dai, H. *Top. Appl. Phys.* **2001**, *80*, 29–53.
(23) Flahaut, E.; Peigney, A.; Bacsa, W. S.; Bacsa, R. R.; Laurent, C. *J. Mater. Chem.* **2004**, *14*, 646–653.
(24) Resasco, D. E.; Alvarez, W. E.; Pompeo, F.; Balzano, L.; Herrera, J. E.; Kitiyanan, B.; Borgna, A. *J. Nanoparticle Res.* **2002**, *4*, 131–136.
(25) Ago, H.; Uehara, N.; Yoshihara, N.; Tsuji, M.; Yumura, M.; Tomonaga, N.; Setoguchi, T. *Carbon* **2006**, *44*, 2912–2918.
(26) Franklin, N. R.; Dai, H. *Adv. Mater.* **2000**, *12*, 890–894.
(27) Endo, M.; Muramatsu, H.; Hayashi, T.; Kim, Y. A.; Terrones, M.; Dresselhaus, M. S. *Nature (London, U.K.)* **2005**, *433*, 476.
(28) Peigney, A.; Coquay, P.; Flahaut, E.; De Grave, E.; Vandenberghe, R. E.; Laurent, C. *J. Phys. Chem. B* **2001**, *105*, 9699–9710.
(29) Hertel, T.; Hagen, A.; Talalaev, V.; Arnold, K.; Hennrich, F.; Kappes, M.; Rosenthal, S.; McBride, J.; Ulbricht, H.; Flahaut, E. *Nano Lett.* **2005**, *5*, 511–514.
(30) Weisman, R. B.; Bachilo, S. M. *Nano Lett.* **2003**, *3*, 1235–1238.
(31) Moon, J.-M.; An, K. H.; Lee, Y. H.; Park, Y. S.; Bae, D. J. *J. Phys. Chem. B* **2001**, *105*, 5677.
(32) Dillon, A. C.; Gennett, T.; Jones, K. M.; Alleman, J. L.; Parilla, P. A.; Heben, M. J. *Adv. Mater.* **1999**, *11*, 1354.
(33) Gregg, S. B.; McKee, K.; Vecchio, S. *J. Phys. Chem. B* **2006**, *110*, 1179.

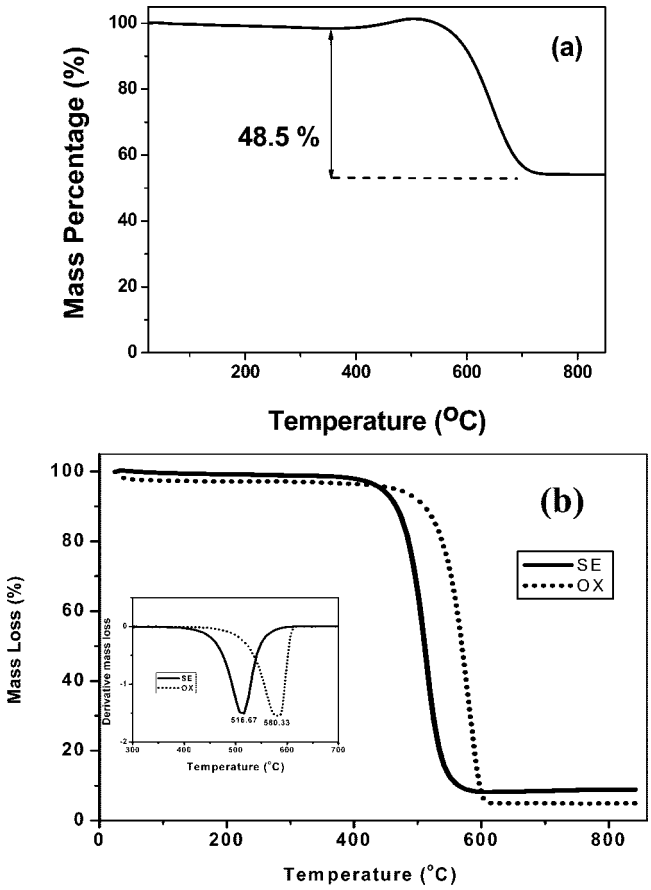

Figure 3. (a) TGA analysis of DWCNT sample as produced and (b) TGA and DTA analysis of DWCNTs before (SE) and after (OX) oxidation. A translation towards a higher thermal decomposition temperature can be observed for the OX sample.

corresponds to the oxidation of the metal catalytic nanoparticles used for the nanotube synthesis process. The remaining quantities left after burning the carbon nanotube products were found to be 9% for SE and 5% for OX and represent oxides of the metallic catalytic nanoparticles that are still present after purification. These conclusions are supported by the DTA profiles that also indicate the presence of only one phase and the analysis of the surface area of the two peaks.[18] The purity for the samples was estimated to be 91% for SE and 95% for OX.

Since no oxidizing acid was used for the catalyst's elimination, one can assume that the amounts of amorphous carbon are the same for the AP and SE samples, a fact that was observed also experimentally. Quantifying the mass loss in the 300−400 °C thermal interval,[34,35] which corresponds to the decomposition of amorphous carbon, it was concluded that the level of amorphous carbon in these two samples is between 0.1 and 0.5 wt %. The lack of amorphous carbon formed in this process can be explained by the lower level of methane self-pyrolysis, which usually occurs in thermal cCVD processes due to the high reaction temperatures, and for the cold-walled RF-cCVD process, the only hot areas are the graphite receptacle and the catalyst system. The burning temperature of 580.3 °C for the OX sample is very close to the values reported in the literature for DWCNTs.[27] The higher burning temperature of the OX sample as compared to the one for the SE sample (516.7 °C) can be attributed to the metallic impurities decrease after oxidation and acid treatment, given that these impurities act as initiation points for the oxidation reaction.[36,37] Most of the metallic impurities were found to be Mo (which is more difficult to remove by acid treatments) and traces of Fe, in good agreement with previous research.[38] These impurities represent the nanoparticles entrapped between the nanotube bundles and that therefore had low exposure to acid. In parallel experiments, it was found that a combination of acid cleaning and continuous sonication to break the nanotube bundles could expose the metallic nanocatalyst particles to acid, resulting in higher overall sample purities.

For SWCNTs and DWCNTs, the Raman spectra contained bands in two characteristic spectral regions: a low wavenumber range (100−400 cm^{-1}), or the radial breathing mode (RBM) region, and a high wavenumber domain between 1200 and 3000 cm^{-1}, or the region of the longitudinal and tangential modes. The position and presence of Raman bands between 100 and 400 cm^{-1} (RBM) strongly depend on the diameter and chirality of the nanotubes.[39,40] The bands that are present in the high-frequency region are band D, positioned between 1250 and 1450 cm^{-1}, associated with vacancies and the presence of other carbonaceous impurities (amorphous carbon, glassy carbon, etc.) that destroy the graphitic symmetry; band G (between 1500 and 1600 cm^{-1}), corresponding to the splitting of the E_{2g} stretching mode for graphite; and the 2D band (between 2450 and 2650 cm^{-1}), which is the second-order harmonic of the D band and is associated with the degree of crystallinity of the graphitic layers.[41,42] Generally, the ratio between the intensity of the G and the D bands (I_G/I_D) can be used to show the presence of structural defects and carbonaceous products with noncrystalline properties.[32] Figure 4 shows the Raman spectra of the SE sample for the two spectral regions.

Since TEM observations have revealed that most of the nanotubes are bundled, this results in a shift in the RBM peak positions as compared to isolated nanotubes. To calculate the nanotube diameters, the following relationship was used: $\omega_{RBM} = (C_1/d) + C_2$, where ω_{RBM} is the RBM frequency (cm^{-1}), d is the nanotube diameter (nm), and C_1 (234) and C_2 (10) are constants that depend upon the excitation energy and bundle

(34) Arepalli, S.; Nikolaev, P.; Gorelik, O.; Hadjiev, V. G.; Holmes, W.; Files, B.; Yowell, L. *Carbon* **2004**, *42*, 1783.
(35) Ramesh, P.; Okazaki, T.; Sugai, T.; Kimura, J.; Kishi, N.; Sato, K.; Ozeki, Y.; Shinohara, H. *Chem. Phys. Lett.* **2006**, *418*, 408.
(36) Hu, H.; Zhao, B.; Itkis, M. E.; Haddon, C. *J. Phys. Chem. B* **2003**, *107*, 13838.
(37) Lee, Y. D.; Lee, H. J.; Han, J. H.; Yoo, J. E.; Lee, Y.-H.; Kim, J. K.; Nahm, S.; Ju, B.-K. *J. Phys. Chem. B* **2006**, *110*, 5310–5314.
(38) Li, Z.; Biris, A. S.; Dervishi, E.; Saini, V.; Xu, Y.; Biris, A. R.; Lupu, D. *J. Chem. Phys.* **2007**, *127*, 154713.
(39) Harutyunyan, A. R.; Pradhan, B. K.; Chang, J.; Chen, G.; Eklund, P. C. *J. Phys. Chem. B* **2002**, *106*, 8671–8675.
(40) Dresselhaus, M. S.; Dresselhaus, G.; Saito, R.; Jorio, A. *Phys. Rep.* **2005**, *409*, 47–99.
(41) Dresselhaus, M. S.; Dresselhaus, G.; Jorio, A.; Souza Filho, A. G.; Saito, R. *Carbon* **2002**, *40*, 2043.
(42) Belin, T.; Epron, F. *Mater. Sci. Eng., B* **2005**, *119*, 105.

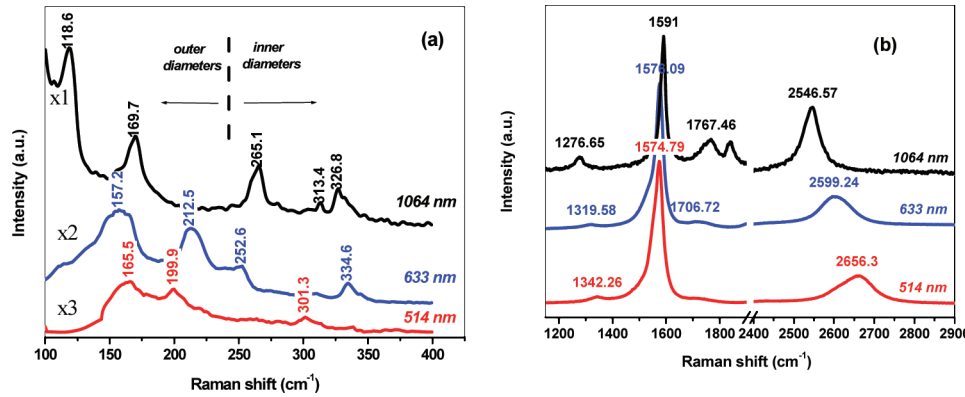

Figure 4. Raman analysis spectra of the low (a) and high (b) frequency domains, which indicate the presence of all the corresponding bands for DWCNTs. Spectra were collected with three laser excitations: 514, 633, and 1064 nm, respectively.

Table 1. Spectral Position and Corresponding Diameter Values of Raman Peaks Collected with Three Laser Excitations

λ_{exc} (nm)	ω_{RBM} (cm^{-1})	d (nm)
514	147.2; 165.5; 199.9; 301.2	1.7; 1.5; 1.23; 0.8
633	133.2; 157.2; 212.5; 252.6; 334.6	1.9; 1.59; 1.15; 0.96; 0.72
1064	106.8; 118.6; 169.7; 265.1; 313.4; 326.8	2.42; 2.15; 1.46; 0.92; 0.77; 0.74

Table 2. Position and Relative Intensity Ratios of D, G, and 2D Bands Present in Raman Spectra Collected at Three Different Laser Excitations for DWCNTs That Are Presented in This Study

λ_{exc} (nm)	ω_D (cm^{-1})	ω_G (cm^{-1})	ω_{2D} (cm^{-1})	I_G/I_D	I_G/I_{2D}
514 (2.41 eV)	1342.3	1574.8	2656.3	31	5.5
633 (1.96 eV)	1319.6	1576.1	2599.2	54	5.5
1064 (1.16 eV)	1276.7	1591	2546.6	14	2.6

sizes.[43,44] The main RBM peaks and the corresponding diameters as calculated using the formula for the three laser excitations are presented in Table 1.

The dominant diameter distribution ranged from 2.42 and 0.72 nm. Taking into consideration that the distance between the walls of the nanotubes varies from 0.335 to 0.42 nm,[45] several diameter combinations were found to be possible. The diameter pairs of the nanotubes identified by HRTEM also were reflected in the diameter range obtained by Raman spectroscopy. Since the TEM analysis indicated the presence of both bundled as well as individual nanotubes, the diameters of the isolated DWCNTs shown in Figure 2c were calculated by the relationship $\omega_{RBM} = (248/d)$,[43] and the ω_{RBM} values corresponding to the external diameter were found to be 106.8 cm^{-1} (1064 nm) and 157.2 cm^{-1} (633 nm). Additionally, both RBM modes corresponding to the internal diameters are shown in Figure 4a. The main Raman characteristics in the high-frequency domain (Figure 4b) are presented in Table 2.

Both Table 2 and Figure 4b highlight the dispersive character of the D and 2D bands as a function of the excitation energy. The shift of the D band of 52 cm^{-1}/eV is the same as the one previously reported for SWCNT bundles.[46] The lower I_G/I_D value for the 1064 nm excitation is probably due to the fact that the larger diameter nanotubes (most probably the outer nanotubes) excited by this laser radiation contain more structural defects as compared to the thinner diameter nanotubes. This has previously been reported in the literature.[47] One can also observe an upshift in the G band by 16 cm^{-1} for the 1064 nm excitation as compared to the 514 and 633 nm excitations. A similar shift (17 cm^{-1}) was previously observed for the 785 nm excitation when compared to the 514 and 633 nm excitations.[45]

Raman analysis of the DWCNT 2D bands (which are not related to the wall defects but to a two-phonon second-order resonance Raman process) were found to be the result of overlapping two distinctive bands (2D) corresponding to the internal diameters (lower frequencies) and to the exterior diameters (superior frequencies), and both show a dispersive character. The laser excitation energies were found to induce changes in the two 2D band spectral positions (being shifted by 37−55 cm^{-1}) and their corresponding intensities.[48,49] Figure 5 presents the 2D regions of the Raman spectra for the DWCNTs synthesized on the Fe−Mo/MgO catalyst and collected at three excitation energies of 1.16 eV (1064 nm), 1.96 eV (633 nm), and 2.41 eV (514 nm). Experimental data show that the 2D band for all excitation energies can be decomposed into two Lorentzian curves with intensities depending upon the excitation energy. This is the result of the selective resonant excitation of various diameters as a function of excitation energy. Their dispersive nature is illustrated in the Figure 5 inset, which shows a linear dependence of the positions corresponding to the two bands as a function of E_{laser}, a relationship that was fitted by the following equation: $\omega_{2D} = \alpha + \beta E_{laser}$, with $\alpha = 2403$ cm^{-1} and $\beta = 95$ cm^{-1}/eV for the inner nanotubes and $\alpha = 2428$ cm^{-1} and $\beta = 101$ cm^{-1}/eV for the outer nanotubes. A small variation between the frequency differences corresponding to the outer and inner nanotubes was observed, and this variation decreased slightly for the lower excitation energies, having a value of 36 cm^{-1} for 1.96 eV, a value that is close

(43) Jorio, A.; Pimenta, M. A.; Souza Filho, A. G.; Saito, R.; Dresselhaus, G.; Dresselhaus, M. S. *New J. Phys.* **2003**, *5*, 13.
(44) Kuzmany, H.; Plank, W.; Hulman, M.; Kramberger, C.; Grü neis, A.; Pichler, T. *Eur. Phys J. B* **2001**, *22*, 307–320.
(45) Wei, J.; Jiang, B.; Zhang, X.; Zhu, H.; Wu, D. *Chem. Phys. Lett.* **2003**, *376*, 753–757.
(46) Dresselhaus, M. S.; Eklund, P. C. *Adv. Phys.* **2000**, *49*, 705–814.
(47) Ago, H.; Nakamura, K.; Imamura, S.; Tsuji, M. *Chem. Phys. Lett.* **2004**, *391*, 308–313.
(48) Kalbáè, M.; Kavan, L.; Zukalová, M.; Dunsch, L. *Carbon* **2004**, *42*, 2915–2920.
(49) Pfeiffer, R.; Kuzmany, H.; Simon, F.; Bokova, S. N.; Obraztsova, E. *Phys. Rev. B: Condens. Matter Mater. Phys.* **2005**, *71*, 155409.

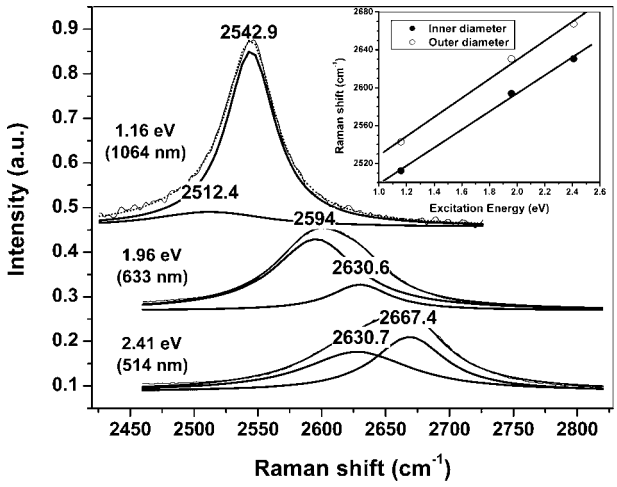

Figure 5. Analysis of the 2D peaks present in the Raman spectra collected using various excitation wavelengths. Each of the peaks can be deconvoluted into two peaks, corresponding to the inner and outer nanotubes forming the double-walled nanotubes. The inset shows the variation of the Raman shift with the excitation energy of the lasers for the inner and outer diameters.

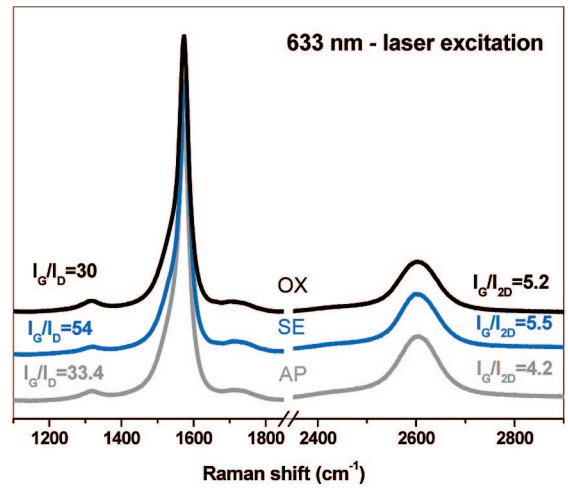

Figure 6. Raman spectra for the higher frequency domain of the double-walled nanotube samples (AP, SE, and OX) exposed to different purification processes. The D, G, and 2D bands along with the ratios between their relative intensities are also shown.

to the ones reported in the literature.[48] The value of β corresponding to the exterior tubes is also in good agreement with the value of 106 cm^{-1}/eV reported for bundled single walls.[46]

Raman spectroscopy also was utilized to evaluate the quality of the nanotubes at different stages of purification. For the 514 and 633 nm excitations, no significant changes were observed in the position and intensity values of the RBM peaks of samples AP, SE, and OX. The Raman spectra for the high-frequency domains at 633 nm excitation, along with the values of the ratios I_G/I_D and I_G/I_{2D}, are presented in Figure 6. A significant observation is the decrease of the I_G/I_D value after oxidation, which indicates that the oxidation process introduced defects in the walls of the nanotubes.[35] However, it is worth mentioning that these damaged CNTs can be potentially rehealed by thermal treatment in argon at 800−1100 °C.[50] The formation of nondetectable amounts of amorphous carbon is explained by the very efficient transformation of the carbon source into the graphitic structures forming the walls of the carbon nanotubes. Similar results have been shown before for the growth of multiwalled carbon nanotubes.[51]

Conclusion

We synthesized via cold-walled RF-cCVD on a novel Fe−Mo/MgO (1:0.2:12.6 wt %) catalyst high-quality DWCNTs with homogeneous inner nanotubes and with outer diameters of 2 nm. The high quality and overall high purity was confirmed by TGA, which revealed a nanotube purity higher than 95% (after purification), and by the I_G/I_D ratio from resonance Raman spectroscopy, we concluded that there was a negligible amount of amorphous carbon and few structural defects in the nanotubes. It was found that post-treatment can strongly affect the properties of the DWCNTs. The acid and oxidation treatment can significantly improve the tube crystallinity as indicated by the high combustion temperature in TGA and the higher G/D band intensity ratio. The reason for the absence of amorphous carbon is probably due to the fact that the self-pyrolysis of the carbon source is kept to a minimum in the inductive heating process. Thus, the carbon source is only decomposed catalytically in the presence of the (heated) metal catalyst to form the highly ordered graphitic layers that compose the carbon nanotubes. Therefore, this method, in conjunction with the Fe−Mo/MgO (1:0.2:12.6 wt % coprecipitation) catalyst, represents a very promising industrial process to produce high-quality DWCNTs on a large scale and at a low cost.

Acknowledgment. This work was partially supported by a U.S. Department of Energy grant (Grant No. DE-FG 36-06 GO 86072).

CM703680N

(50) Chattopadhyay, D.; Galeska, I.; Papadimitrakopoulos, F. *Carbon* **2002**, *40*, 985–988.
(51) Biris, A. S.; Schmitt, T. C.; Little, R. B.; Li, Z.; Xuv, Y.; Biris, A.R.; Lupu, D.; Dervishi, E.; Trigwell, S.; Miller, D. W.; Rahman, Z. *J. Phys. Chem.* **2007**, *111*, 17970–17975.